Interaction Notes
Note 580
10 February 2003

Exploiting Early Time Response Using the Fractional Fourier Transform for Target Identification

[*]Seongman Jang, [*]Tapan K. Sarkar, [*] Kyungjung Kim, [**]Carl E. Baum
[*] Department of Electrical Engineering and Computer Science
Syracuse University, 121 Link Hall, Syracuse, NY 13244
**** Air Force Research Laboratory, Directed Energy Directorate, Kirtland Air Force Base, New Mexico**

Abstract – This paper presents a new technique for estimating parameters of damped sinusoids utilizing both early and late time transient scattering responses. Transient scattering responses are composed of damped sinusoids at late times and impulse-like components at early times. Due to the impulse-like components, it is difficult to extract meaningful damped sinusoids when analyzing the complete data set. In this paper, the entire time domain response is used to extract the signal parameters of interest utilizing both the early and late times. The fractional Fourier transform (FrFT), especially the half Fourier transform (HFT) is used to analyze the data for parameter identification. Impulse or Gaussian-like pulses can be easily separated from the damped exponentials in the HFT domain, as they have similar functional representations. Results from several examples show that the new technique is applicable for signals that are composed of damped exponentials and short pulse-like components.

This work was supported in part by the Air Force Office of Scientific Research, and in part by the Air Force Research Laboratory, Directed Energy Directorate, Kirtland Air Force Base, New Mexico.

1. Introduction

1.1. Problem Statement

In order to characterize an unknown object by remote sensing, certain electrical properties of the object may be used. In particular the impulse response, ramp response, and the natural resonant frequencies of the object have been proposed [1-4]. To identify an object accurately, one must illuminate it with a band of frequencies whose wavelengths must at least contain components which are approximately the same dimensions as the overall length of the object. Since, in general, the size of an object is not known beforehand, it is necessary to illuminate the object by a broadband signal such as a waveform which is an approximation to an impulse. The transmitted pulse induces electrical currents on the object and these currents reradiate the incidental energy. The goal here is to obtain the electrical properties of the object from the transmitted and received time domain waveforms. Because the complex poles are aspect independent, they are suitable for target identification/classification. The resonant frequencies of a conducting object can be used as a signature for that object to discriminate it from others for the purpose of target identification.

1.2. Theory

The singularity expansion method (SEM) proposed by Baum [5] has been applied to express electromagnetic response in an expansion of complex resonances of the system [6]. It has been shown that the dominant complex natural resonances of a system are a minimal set of parameters that define the overall physical properties of the system [7]. So, a transient scattering response is analyzed in terms of the damped oscillations corresponding to the complex resonant frequency of the scatterer or target. In general, the signal model of the observed late time of an electromagnetic-energy-scattered response from an object can be written as

$$y(t) = x(t) + n(t) \approx \sum_{m=1}^{M} R_m \exp(s_m t) + n(t); \quad 0 \le t \le T, \tag{1}$$

where $y(t)$ = observed time domain response,

$n(t)$ = noise in the system,

$x(t)$ = signal,

R_m = residues or complex amplitudes,

$s_m = -\alpha_m + j\omega_m$,

α_m = damping factors,

ω_m = angular frequencies ($\omega_m = 2\pi f_m$).

After sampling, the time variable, t is replaced by kT_s, where T_s is the sampling period. The original continuous time sequence can be rewritten as

$$y(kT_s) = x(kT_s) + n(kT_s) \approx \sum_{m=1}^{M} R_m z_m^k + n(kT_s) \text{ for k} = 0, \ldots, N-1, \quad (2)$$

$$z_m = e^{s_i T_s} = e^{(-\alpha_m + j\omega_m)T_s} \text{ for m} = 1, 2, \ldots, M. \quad (3)$$

Since the resonance describe global wave fields that encompass the scattering object as a whole, the SEM series representation encounters convergence difficulties at early times when portions of the objects are not yet excited. Early time response is strongly dependent on the nature of the source, the location of the source, and the location of the observer. Usually the early time response shows impulse-like characteristics. Because of this difficulty, most previous techniques used just late time signals only.

The most well-known pole retrieval method is Prony's method [7-11], which was applied first by Van Blaricum and Mittra [8, 10], to the electromagnetic transient problem. This method has also received a great deal of attention in the signal processing community. Study of this method has resulted in its improved and generalized versions [11] and understanding of their noise perturbation properties [12, 13]. Prony's method has been applied with success where analyzing measured impulse responses with high signal-to-noise ratio. However it is difficult to extend Prony's method to arbitrary input and arbitrary output waveforms because Prony's method can be very sensitive to noise and requires an *a priori* selection of the model order. Also the SEM representation does not account for the impulsive portion of the early time system responses behavior. Another well-known method for pole extraction is the pencil-of function method [12-15] whose application to radar transient waveform identification was presented initially by Sarkar et al. [14]. Recent applications of the pencil-of-functions method have been found in improved and generalized forms [15, 16]. A generalized pencil-of function method, termed as the Matrix Pencil

Method (MPM), overcomes the disadvantages of the Prony's method. It is robust to noise and does not require an *a priori* knowledge of the model order. But, since it is hard to know a-priori where the early time response ends and late time starts, it is not easy to apply either the Prony's method or the Matrix pencil method.

Deficiencies in the representation of the early time signal, can be repaired by inclusion of an 'entire function' in the complex frequency domain or in the choice of the 'coupling coefficients'. The use of time-dependent coupling coefficients has been proposed as a means of describing the early time scattering response [17, 18]. The approach used by Morgan [18] was to separate the solution from the magnetic field integral equation (MFIE) into its physical optics and natural mode terms. It was shown that the transient quantities could be described as a sum of physical optics components along with the modal expansion terms. Although several authors have investigated the various coupling coefficients in analytical developments and in the calculation of currents on the scatterer, their results for scattered fields have been limited [19, 20]. And Felsen argues that the method is formally correct [21], because it is necessary to include entire functions rather than coupling coefficients to describe early time response. Baum developed a method for bounding the extent of the entire function (which has no singularities in the entire s plane, i.e., the Laplace transform plane) [22] in its temporal form. A Gaussian pulse is one such example of the entire functions. Another technique that has been suggested for the computation of the entire function is that of the geometrical theory of diffraction (GTD) [23]. This method yields a high-frequency approximation to the solution of Maxwell's equations [24]. Furthermore, after the ray tracing is performed, all pertinent distances between the source and target are known, so time gating can be used to enforce causality. As the scattering process progresses in time, the ray tracing associated with multiple bounce diffraction becomes very complicated, and therefore places a bound on the time interval beyond which the method may be employed. Also in the late times the coupling tends to be associated with lower spectral content, for which the GTD was never intended.

In this paper, the transient electromagnetic response is considered in the time domain and in the fractional Fourier Transform (FrFT) domain consisting of the entire data set. Fractional Fourier transform (FrFT) is a generalized Fourier transform. Using the FrFT it is possible to discriminate an impulse or a Gaussian pulse from the other components of the

signals. Because of this property, impulse-like early time components can be separated from the damped exponentials. To describe the early time response a Gaussian pulse is selected. A Gaussian pulse is an entire function [22] and is quite adequate to describe pulse-like components in early time. Complex exponentials are used to describe the late time signals. The concept of a 'Turn-on time' [25] is utilized to consider a time when the fully excited resonance can be used, formally. In this study a Quasi-Newton approach augmented by a model trust strategy is used to optimize the parameters. Initial guess for the damped exponentials were determined by the Matrix pencil method (MPM).

In section II, the definition and some properties of a fractional Fourier transform (FrFT) are presented. Half Fourier transform (HFT) is introduced as a special case of FrFT and also FrFT and HFT of some functions are tabulated. Fractional Fourier transform of a causal damped exponential is derived. Method for obtaining the FrFT of an arbitrary input signal is introduced in section III. Optimization technique that is chosen in this research is briefly discussed in section IV. Some examples are given in section V and concluding remarks are followed.

2. Fractional Fourier Transform (FrFT)

Victor Namias proposed a fractional order Fourier transform using Hermite polynomials in 1980, which is called a Fractional Fourier transform (FrFT) [20].

$$F_\alpha\left\{ e^{-x^2/2} H_n(x) \right\} = e^{-jn\alpha} e^{-x^2/2} H_n(x) \qquad (4)$$

where F_α is a Fourier transform operator, α is a continuous transformation parameter and $H_n(x)$ are the Hermite polynomials of order n. It can be shown that the Hermite polynomials are eigenfunctions of the Fourier transform operator F_α and its eigenvalues are $e^{-jn\alpha}$. (Actually, Namias used the mathematical definition of the Fourier transform rather than the engineering definition. But in this research we will use the engineering definition of Fourier transform as presented in Equation 4.) Later A. C. McBride and F. H. Kerr made Victor Namias' definition more clear and rigorous [26]. Luis B. Almeida used the engineering convention of Fourier transform to define FrFT and represented FrFT as a

rotation in the time-frequency plane [27]. Almeida's convention for FrFT and FT are used in this paper, so that, a Fourier transform pair of a $x(t)$ is defined as,

$$F_{\pi/2}\{x(t)\}(\omega) = X(\omega) = \frac{1}{\sqrt{2\pi}}\int_{-\infty}^{\infty} x(t)\, e^{-j\omega t}\, dt \tag{5-1}$$

$$F_{-\pi/2}\{X(\omega)\}(t) = x(t) = \frac{1}{\sqrt{2\pi}}\int_{-\infty}^{\infty} X(\omega) e^{j\omega t}\, dt \tag{5-2}$$

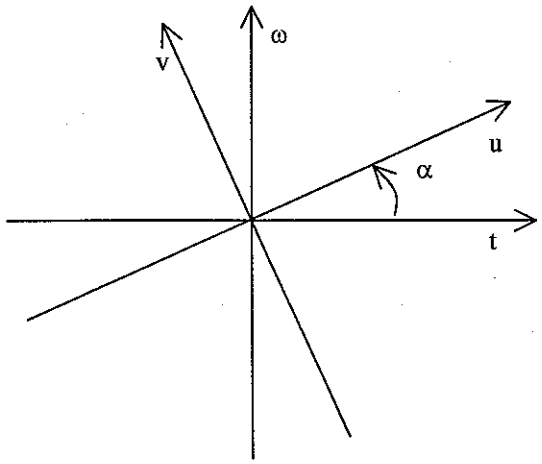

Figure 1. Description of the Time-Frequency plane and a set of coordinates (u,v) rotated by an angle α relative to the original coordinates (t,ω).

The Fourier Transform of a signal can be interpreted as a π/2 angular rotation of the signal in the Time-Frequency plane. The FrFT is then developed and interpreted as the rotation of a signal to any angle α with the time axis in the time-frequency plane as shown in Figure 1 [27]. It is known that the operation $F_{\pi/2}$ and $F_{-\pi/2}$ are complex conjugates of each other and they satisfy the relations $F_{\pi/2}F_{-\pi/2} = F_{-\pi/2}F_{\pi/2} = 1$. Also note that,

$$F_{\pi/2}x(t) = X(\omega) \tag{6-1}$$

$$F_{\pi}x(t) = F_{\pi/2}X(\omega) = x(-t) \tag{6-2}$$

$$F_{3\pi/2}x(t) = F_{\pi/2}x(-t) = X(-\omega) \tag{6-3}$$

$$F_{2\pi}x(t) = F_{\pi/2}X(-\omega) = x(t) \tag{6-4}$$

Generally, the additivity property of a fractional Fourier transform operator holds, that is,

$$F_{\alpha} + F_{\beta} = F_{\alpha+\beta}. \tag{7}$$

The FrFT is a linear transform defined by means of the transformation kernel as [27],

$$K_\alpha(t,u)=\begin{cases}\sqrt{\dfrac{1-j\cot\alpha}{2\pi}}e^{j\frac{t^2+u^2}{2}\cot\alpha-jut\csc\alpha} & \text{if } \alpha \text{ is not a multiple of } \pi\\ \delta(t-u) & \text{if } \alpha \text{ is not a multiple of } 2\pi\\ \delta(t+u) & \text{if } \alpha+\pi \text{ is not a multiple of } 2\pi\end{cases} \quad (8)$$

where $j=\sqrt{-1}$ and α is the rotation angle of a transformed signal . The kernel has the following properties,

$$K_\alpha(t,u)=K_\alpha(u,t) \quad (9)$$

$$K_{-\alpha}(t,u)=K_\alpha^*(t,u) \quad (10)$$

$$K_\alpha(-t,u)=K_\alpha(t,-u) \quad (11)$$

$$\int_{-\infty}^{\infty}K_\alpha(t,u)K_\beta(u,z)du=K_{\alpha+\beta}(t,z) \quad (12)$$

$$\int_{-\infty}^{\infty}K_\alpha(t,u)K_\alpha^*(t,u')dt=\delta(u-u') \quad (13)$$

The forward and backward FrFTs are defined as

$$(F_\alpha x)(u)=X_\alpha(u)=\int_{-\infty}^{\infty}x(t)K_\alpha(t,u)dt \quad (14\text{-}1)$$

$$(F_{-\alpha}X)(t)=x(t)=\int_{-\infty}^{\infty}X_\alpha(u)K_{-\alpha}(t,u)du. \quad (14\text{-}2)$$

So, if α is not a multiple of π, the FrFT is defined as,

$$X_\alpha(u)=\sqrt{\frac{1-j\cot\alpha}{2\pi}}e^{j\frac{u^2}{2}\cot\alpha}\int_{-\infty}^{\infty}x(t)e^{j\frac{t^2}{2}\cot\alpha}e^{jut\csc\alpha}dt. \quad (15)$$

Thus the computation of the FrFT can be understood from the following steps: 1) multiply the signal by a chirp, 2) take the Fourier transform with its argument scaled by $\csc\alpha$, 3) then another product is taken with a chirp, 4) this product is scaled by a complex amplitude factor. From Equation (14-2), the FrFT consists of expressing $x(t)$ using a basis formed by the set of functions $K_{-\alpha}(u,t)$ (with u acting as a parameter for spanning the set of basis functions). The basis functions are chirps, i.e. complex exponentials with linear frequency modulation and they are orthonormal, according to equation (13). A number of important properties of the FrFT and their proofs can be found in [27]. Those properties are extensions

of the corresponding properties of the Fourier transform. Table 1 gives the half Fourier transform of a number of special functions. The half Fourier transform is a special case of FrFT when $\alpha = \pi/4$.

Table 1. Half Fourier Transform (HFT) of some special functions (Here, n = 0, 1, 2,..., an integer, u is the HFT domain variable, c is a constant, and $H_n(u)$ is the n[th] order Hermite polynomial).

Eqn. No.	Signal	HFT, $\alpha=\pi/4$
(16)	$\delta(t)$	$\sqrt{\frac{1-j}{2\pi}}e^{j\frac{u^2}{2}}$
(17)	$\delta(t-\tau)$	$\sqrt{\frac{1-j}{2\pi}}e^{-\frac{j}{2}\tau^2}e^{\frac{j}{2}(u-\sqrt{2}\tau)^2}$
(18)	1	$\sqrt{1+j}\,e^{-j\frac{u^2}{2}}$
(19)	e^{jvt}	$\sqrt{1+j}\,e^{\frac{j}{2}v^2}e^{-\frac{j}{2}(u-\sqrt{2}v)^2}$
(20)	$e^{jc\frac{t^2}{2}}$	$\sqrt{\frac{1+j}{1+c}}\,e^{j\frac{u^2}{2}\frac{c-1}{c+1}}$
(21)	$e^{-\frac{t^2}{2}}$	$e^{-j\frac{u^2}{2}}$
(22)	$H_n(t)e^{-\frac{t^2}{2}}$	$e^{-jn\pi/4}H_n(u)e^{-\frac{u^2}{2}}$
(23)	$e^{-c\frac{t^2}{2}}$	$\sqrt{\frac{1-j}{c-j}}\exp\left\{\frac{ju^2}{2}\frac{c^2-1}{c^2+1}\right\}\exp\left\{-\frac{u^2}{2}\frac{2c}{c^2+1}\right\}$
(24)	$e^{-c\frac{(t-\tau)^2}{2}}$	$\sqrt{\frac{1-j}{c-j}}\exp\left\{-\frac{c}{c^2+1}\left(u-\frac{\tau}{\sqrt{2}}\right)^2\right\}\exp\left\{\frac{j}{2}\left[\frac{c^2-1}{c^2+1}\left(u-\frac{\tau}{\sqrt{2}}\right)^2+\frac{\tau^2}{2}-\sqrt{2}u\tau\right]\right\}$

In this paper, the Half Fourier transform is used for parameter optimization. There are many impulse-like components at an early time of a scattered transient response. It is very difficult to separate each impulse-like component in the time domain. But it is possible to tell when those pulses occur in the half Fourier transform domain because HFT of an impulse and a Gaussian pulse, equation (17) and (24), have much more information about time when they first appear.

Figure 2 shows the Fourier transform and the half Fourier transform of a shifted impulse $\delta(t-2)$. Figure 3 shows the same for a shifted Gaussian pulse. It is clear that HFT of those pulses have the information about time history when they first appear. That is, around the pulse position in the HFT domain ($u = 2$ *and* 5), the linear phase property breaks down.

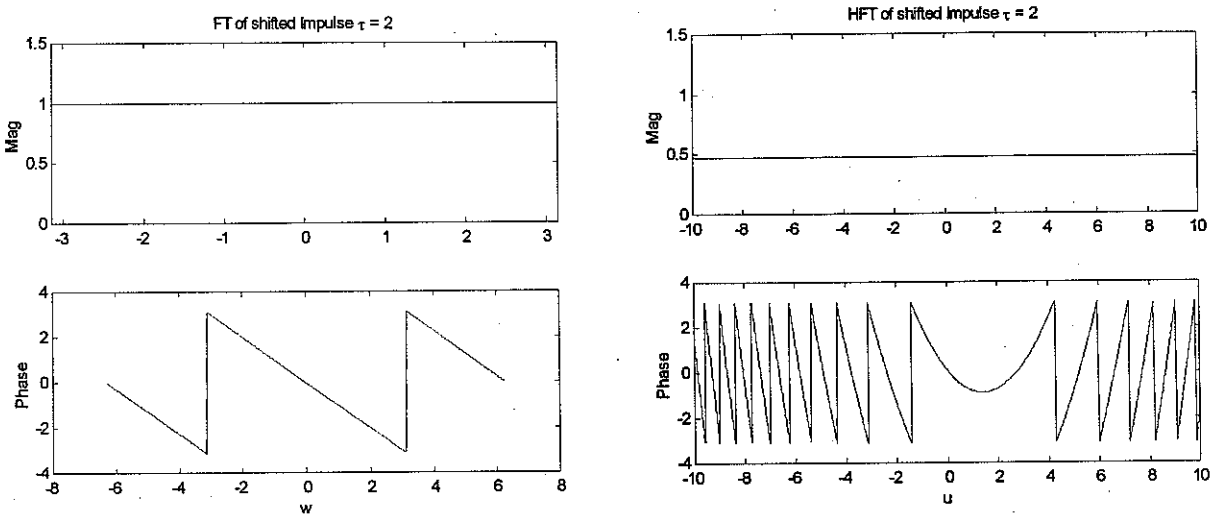

(a) Fourier transform (FT)

(b) Half Fourier transform (HFT)

Figure 2. FT and HFT of a shifted impulse $\delta(t-2)$.

Components such as an impulse or a Gaussian pulse can be used to characterize the early time representations and the complex exponentials to approximate late time responses. But their functional representations are almost the same in the half Fourier transform domain. It is clear from (17) and (19) that the HFT of the shifted impulse and that of the damped exponential have similar functional representation, except that the coefficient and the sign of the power of the exponent. So it is possible to separate the impulse-like component in the half Fourier transform domain quite easily.

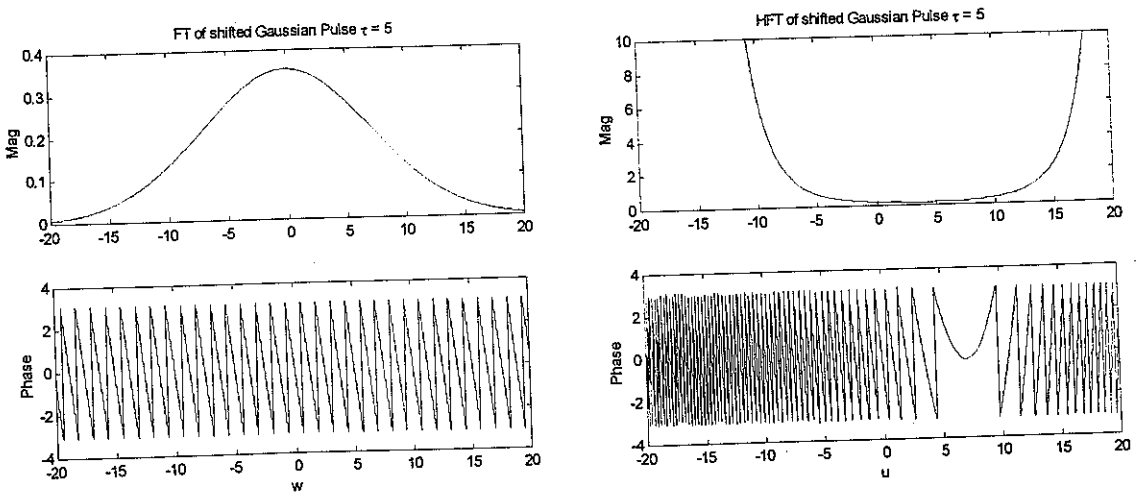

(a) Fourier transform (FT)

(b) Half Fourier transform (HFT)

Figure 3. FT and HFT of a shifted Gaussian pulse $e^{-50\frac{(t-5)^2}{2}}$.

Usually signals that we encounter in real life are causal, that is, $x(t) = 0$ if $t \le 0$. And the initial time as to when a resonant component starts is different from component to component. So it is possible to assume that each resonant component has a different 'turn-on time'. In this study the phrase 'turn-on time' is the time when each resonant component can be used formally to represent the temporal data. To apply FrFT to those causal signals we present some formulas in Table 2. The detailed derivation of the FrFT of a function (26) described in shown next.

Table 2. HFT of some causal functions for $t > 0$. (Here v is complex, $u(t)$ is a unit step function, u is a variable in the fractional Fourier transform domain, $\beta = j/2$, and $\Phi(z) = \frac{1}{\sqrt{2\pi}} \int_0^z e^{-\lambda^2/2} d\lambda$ and $t > 0$, $a > 0$.)

Eqn	Signal	HFT, $\alpha=\pi/4$
(25)	$e^{jvt}u(t)$	$\frac{\sqrt{1+j}}{2} e^{\frac{j}{2}v^2} \exp\left\{-\frac{j}{2}\left(u-\sqrt{2}v\right)^2\right\}\left[1-\Phi\left(\gamma\sqrt{\beta}\right)\right]$, $\gamma = j\left(\sqrt{2}u - v\right)$
(26)	$e^{jvt}u(t-\tau)$	$\frac{\sqrt{1+j}}{2} e^{\frac{j}{2}v^2} \exp\left\{-\frac{j}{2}\left(u-\sqrt{2}v\right)^2\right\}\left[1-\Phi\left(\gamma'\sqrt{\beta}\right)\right]$, $\gamma' = j\left(\sqrt{2}u - v - \tau\right)$
(27)	$e^{jv(t-\tau)}u(t-\tau)$	$\frac{\sqrt{1+j}}{2} e^{-jv\tau} e^{\frac{j}{2}v^2} \exp\left\{-\frac{j}{2}\left(u-\sqrt{2}v\right)^2\right\}\left[1-\Phi\left(\gamma'\sqrt{\beta}\right)\right]$, $\gamma' = j\left(\sqrt{2}u - v - \tau\right)$

For the signal $x(t)=e^{jvt}u(t-\tau)$, we have $u(t-\tau)$ is a unit step function and τ is a 'Turn-on time'. By using the definition of the fractional Fourier transform (15), we obtain

$$X_\alpha(u)=\sqrt{\frac{1-j\cot\alpha}{2\pi}}e^{\frac{j}{2}u^2\cot\alpha}\int_{-\infty}^{\infty}x(t)\exp\left\{\frac{j}{2}t^2\cot\alpha-jut\csc\alpha\right\}dt \tag{28}$$

$$=\sqrt{\frac{1-j\cot\alpha}{2\pi}}e^{\frac{j}{2}u^2\cot\alpha}\int_{-\infty}^{\infty}\exp\left\{-\left[-\frac{j}{2}\cot\alpha\right]t^2-j(u\csc\alpha-v)t\right\}dt$$

We set $\frac{1}{4\beta}=-\frac{j}{2}\cot\alpha$, (so $\beta=\frac{j}{2}\tan\alpha$), and $\gamma=j(u\csc\alpha-v)$, (29)

then

$$X_\alpha(u)=\sqrt{\frac{1-j\cot\alpha}{2\pi}}e^{\frac{j}{2}u^2\cot\alpha}\int_{-\infty}^{\infty}\exp\left\{-\frac{t^2}{4\beta}-\gamma t\right\}dt \tag{30}$$

We now make the change of variable $y=t-\tau$, to yield

$$X_\alpha(u)=\sqrt{\frac{1-j\cot\alpha}{2\pi}}e^{\frac{j}{2}u^2\cot\alpha}\exp\left\{-\frac{\tau^2}{4\beta}-\gamma\tau\right\}\int_{-\infty}^{\infty}\exp\left\{-\frac{y^2}{4\beta}-\left(\gamma+\frac{\tau}{2\beta}\right)y\right\}dy \tag{31}$$

$$\text{Set } \gamma'=\gamma+\frac{\tau}{2\beta}=j(u\csc\alpha-v)+\frac{\tau}{j\tan\alpha}=j(u\csc\alpha-v-\tau\cot\alpha), \tag{32}$$

then ,

$$X_\alpha(u)=\sqrt{\frac{1-j\cot\alpha}{2\pi}}e^{\frac{j}{2}u^2\cot\alpha}\exp\left\{-\frac{\tau^2}{4\beta}-\gamma\tau\right\}\int_{-\infty}^{\infty}\exp\left\{-\frac{y^2}{4\beta}-\gamma' y\right\}dy \tag{33}$$

From the integral in Tables [33], Eq. 3.322.2 (p307), we get

$$\int_{-\infty}^{\infty}\exp\left\{-\frac{y^2}{4\beta}-\gamma y\right\}dy=\sqrt{\pi\beta}\exp(\beta\gamma^2)\left[1-\Phi(\gamma\sqrt{\beta})\right] \tag{34}$$

where $\Phi(z)$ is a complex error function. By using (32),(34), one obtains

$$X_\alpha(u)=\frac{\sqrt{1+j\tan\alpha}}{2}e^{\frac{j}{2}u^2\cot\alpha}\exp\left\{-\frac{\tau^2}{4\beta}-\gamma\tau\right\}\exp\left\{\frac{j}{2}\tan\alpha\left(\gamma+\frac{\tau}{2\beta}\right)^2\right\}\left[1-\Phi(\gamma'\sqrt{\beta})\right] \tag{35}$$

Substitute β and γ from (29) into (35) then, after some manipulations, we get

$$X_\alpha(u) = \frac{\sqrt{1+j\tan\alpha}}{2}\exp\left\{-\frac{j}{2}\left[\left(u^2+v^2\right)\tan\alpha - 2uv\sec\alpha\right]\right\}\left[1-\Phi\left(\gamma'\sqrt{\beta}\right)\right] \quad (36)$$

where $v = \omega + j\alpha$, $\gamma' = j(u\csc\alpha - v - \tau\cot\alpha)$, $\beta = \frac{j}{2}\tan\alpha$, a>0. (37)

3. Calculation of the FrFT of an arbitrary input signal

Namias [20] defined the generalized Fourier Transform operator F_α by,

$$F_\alpha\left\{e^{-x^2/2}H_n(x)\right\} = e^{-jn\alpha}e^{-x^2/2}H_n(x) \quad (38)$$

where α is variable parameter, $-\pi \le \alpha \le \pi$, with negative values of α corresponding to the inverse transform and $H_n(t)$ is the n[th] order Hermite polynomial. Therefore, the usual Fourier Transform operator can be written as $F_{\pi/2}$ to denote the eigenvalue $e^{-jn\pi/2}$ associated with the orthogonal Hermite functions $e^{-x^2/2}H_n(x)$. The associate Hermite (AH) polynomials $h_n(t,\lambda)$ are defined in terms of the Hermite polynomials $H_n(t,\lambda)$. [28]

$$h_n(t,\lambda) = \frac{1}{\sqrt{2^n n!\sqrt{\pi}\lambda}}H_n\left(\frac{t}{\lambda}\right)\exp\left(-\frac{t^2}{2\lambda^2}\right), \qquad n \ge 0 \quad (39)$$

where λ is a scaling factor. The Hermite polynomials are generated recursively through

$$h_0(t) = \frac{e^{-\left(t^2/2\right)}}{\sqrt{\sqrt{\pi}}}$$

$$h_1(t) = \frac{2\,t\,e^{-\left(t^2/2\right)}}{\sqrt{2\sqrt{\pi}}} \quad (40)$$

$$h_n(t) = \frac{1}{\sqrt{n}}\left[\sqrt{2}\,t\,h_{n-1}(t) - \sqrt{n-1}\,h_{n-2}(t)\right], \qquad \text{for } n \ge 2$$

The AH polynomials are orthogonal to each other and form a complete set of basis in the interval $[-\infty,\infty]$. If $x(t)$ is a piecewise smooth function in every finite interval $[-p,p]$ and

$$\int_{-\infty}^{\infty} e^{-t^2}x^2(t)dt \quad < \infty, \quad (41)$$

then $x(t)$ can be expanded using the AH series as

$$x(t) = \sum_{n=0}^{\infty} a_n h_n(t), \qquad for \quad -\infty < t < \infty \tag{42}$$

with

$$a_n = \int_{-\infty}^{\infty} x(t) h_n(t) dt \tag{43}$$

Applying (38) to (42) with (43), we can get

$$F_\alpha x(t)(u) = \sum_{0}^{\infty} a_n e^{-jn\alpha} h_n(u). \tag{44}$$

HFT can be obtained by substituting α with $\pi/4$.

4. Optimization

In this section, a brief explanation of the optimization scheme is presented. First modeling of the backward scattered field is shown and then the scheme for the initial guess for the complex exponentials – total least square matrix pencil method (TLS-MPM)- is presented. Initial guesses for the Gaussian pulses are induced from the shape of the time domain function and the structure of the object. The search for optimum parameters proceeds using a quasi-Newton approach, augmented by a model trust strategy.

4.1. Modeling

The backward scattered field of an object or target can be described by the summations of complex exponentials and entire functions. To represent pulse-like early time component, an entire function is needed. Entire functions are a subset of analytic functions that do not have any singularities in the complex plane. In this study a Gaussian pulse is used for early time description. Gaussian pulse is an entire function and time limited [17]. So, it is appropriate to represent superimposed impulse-like signals at early times of a scattered response. Complex natural frequencies occur in complex conjugate pairs and they lie in the left half plane with nonzero real part. To represent real signals we treat two conjugate poles together. So, the scattered field can be represented by equation (45),

$$x(t) = \frac{1}{2} \sum_{m=1}^{M} c_m e^{-\alpha_m t} \left\{ e^{j(\omega_m t + \phi_m)} + e^{-j(\omega_m t + \phi_m)} \right\} u(t - \tau_m) + \sum_{n=1}^{N} A_n \exp\left\{ -C_n \frac{(t - B_n)^2}{2} \right\} \tag{45}$$

where $t \geq 0, \tau > 0, \alpha_m > 0$. c_m's and ϕ_m's are the amplitudes and the phases, respectively. α_m's and ω_m's are the damping factors and the frequencies. A_n's and B_n's are amplitudes and time shift of the Gaussian pulses. C_n's are coefficients which represent the pulse width. M is the number of sinusoidal signals and N is the number of pulses.

To apply a parameter identification algorithm, the set of variables defined by

$$\underline{p} = [\omega_1\ \phi_1\ c_1\ \alpha_1\ \tau_1 \cdots \omega_M\ \phi_M\ c_M\ \alpha_M\ \tau_M\ ;\ B_1\ A_1\ C_1 \cdots B_N\ A_N\ C_N] \tag{46}$$

needs to be solved for. The residual vector or equivalently the error to be minimized is defined by

$$r = \frac{1}{2} \left\| \overline{G}(u) - \overline{G}_M(u,p) \right\|_2^2 \tag{47}$$

where $\overline{G}(u)$ is the HFT of the measured signal , and $\overline{G}_M(u,p)$ is the HFT of the damped sinusoidal model including pulses. The 2-norm $\|\bullet\|_2$ is the usual $\mathcal{L}^2$ norm. From Table I, Eqn. (24) and Table II, Eqn. (26), $\overline{G}_M(u,p)$ is constructed as

$$\begin{aligned}\overline{G}_M(u,p) = \frac{1}{2}\sum_{m=1}^{M} c_m \frac{\sqrt{1+j}}{2} \Bigg\{ & e^{j\phi_m} e^{\frac{j}{2}v_{m1}^2} \exp\left\{-\frac{j}{2}\left(u-\sqrt{2}v_{m1}\right)^2\right\}\left[1-\Phi\left(\gamma'_{m1}\sqrt{\beta}\right)\right] \\ & + e^{-j\phi_m} e^{\frac{j}{2}v_{m2}^2} \exp\left\{-\frac{j}{2}\left(u-\sqrt{2}v_{m2}\right)^2\right\}\left[1-\Phi\left(\gamma'_{m2}\sqrt{\beta}\right)\right]\Bigg\} \\ + \sum_{n=1}^{N} A_n \sqrt{\frac{1-j}{C_n-j}} & \exp\left\{-\frac{C_n}{C_n^2+1}\left(u-\frac{B}{\sqrt{2}}\right)^2\right\} \exp\left\{\frac{j}{2}\left[\frac{C_n^2-1}{C_n^2+1}\left(u-\frac{B}{\sqrt{2}}\right)^2 + \frac{B^2}{2} - \sqrt{2}uB\right]\right\}\end{aligned} \tag{48}$$

where $v_{m1} = b + ja$, $v_{m2} = -b + ja$, $\gamma'_{m1} = j\left(\sqrt{2}u - v_{m1} - \tau_m\right)$ and $\gamma'_{m2} = j\left(\sqrt{2}u - v_{m2} - \tau_m\right)$

4.2. Initial guess using the Total Least Square Matrix Pencil Method

To increase the speed of convergence and to avoid convergence of the optimization method to an undesirable local minimum, good initial guesses for the parameters of interest are important. In this paper, the TLS-MPM is used for computing the parameters of the complex exponentials as initial guesses. The TLS-MPM approach is the most efficient and

robust technique to fit a noisy data with a sum of complex exponentials [29, 30]. To implement TLS-MPM, one forms the data matrix [Y] with input data y as

$$[Y]=\begin{bmatrix} y(0) & y(1) & \cdots & y(L) \\ y(1) & y(2) & \cdots & y(L+1) \\ \vdots & \vdots & & \vdots \\ y(N-L-1) & y(N-L) & \cdots & y(N-1) \end{bmatrix}_{(N-L)x(L+1)} \tag{49}$$

where N is number of data and L is pencil parameter. For efficient noise filtering L is chosen between N/3 to N/2. Then singular value decomposition (SVD) of the matrix [Y] is calculated from

$$[Y]=[U][\Sigma][V^H]. \tag{50}$$

Here, [U] and [V] are unitary matrices, composed of the eigenvectors of $[Y][Y]^H$ and $[Y]^H[Y]$, respectively, and [Σ] is a diagonal matrix containing the singular values of [Y]. At this stage, the number of exponentials is determined by the ratio of the singular values to the largest one. Consider the singular value σ_c such that

$$\frac{\sigma_c}{\sigma_{\max}} \approx 10^{-p}, \tag{51}$$

where p is the number of significant decimal digit in the data. For example, if the data is accurate up to 3 significant digits, then the singular values for which the ratio in above equation is below 10^{-3} are essentially noise singular values, and they should not be used.

Next, consider the 'filtered' matrix, $[V']$, constructed so that it contains only M dominant right singular vectors of [V],

$$[V']=[v_1, v_2, \cdots, v_m]. \tag{52}$$

The right singular vectors from M+1 to L, corresponding to the small singular values, are discarded. Therefore,

$$[Y_1]=[U][\Sigma'][V_1']^H, \tag{53-1}$$

$$[Y_2]=[U][\Sigma'][V_2']^H, \tag{53-2}$$

where $[V_1']$ is obtained from $[V']$ with the last row of $[V']$ deleted, $[V_2']$ is obtained by removing the first row of $[V']$, and $[\Sigma']$ is obtained from the M columns of [Σ]

corresponding to the M dominant singular values. The poles of the signals are given by the non-zero eigenvalues of

$$\left\{[V_1']^H\right\}^{+}[V_2']^H \tag{54}$$

which are the same as the eigenvalues of

$$[V_2']^H\left\{[V_1']^H\right\}^{+} \tag{55}$$

Once M and the poles [$z_i = \exp(-a + jb)T_s$] are known, the residues, R_i, are solved from the following least square problem,

$$\begin{bmatrix} y(0) \\ y(1) \\ \vdots \\ y(N-1) \end{bmatrix} = \begin{bmatrix} 1 & 1 & \cdots & 1 \\ z_1 & z_2 & \cdots & z_M \\ \vdots & \vdots & & \vdots \\ z_1^{N-1} & z_2^{N-1} & \cdots & z_M^{N-1} \end{bmatrix} \begin{bmatrix} R_1 \\ R_2 \\ \vdots \\ R_M \end{bmatrix} \tag{56}$$

5. Examples

In this section, two examples are presented to validate the above technique. One is a wire scatterer and other is a conducting sphere. Analytical values of the poles have been presented by other researchers and are compared with the results of the proposed technique.

5.1 Wire scatterer

The first example is a thin wire scattering element of length L and diameter d which is excited by an incident pulse of electromagnetic radiation. As shown in Figure 4, L, the length of the wire scatterer is 50mm and the aspect ratio (d/L) is 0.01. The incident field is coming from 45 degree from the wire axis and is polarized with respect to the theta direction.

The backward scattered field, shown in Figure 5, has been computed using the electromagnetic analysis code WIPL-D [31], in the frequency domain. The frequency range covered is from 0.2 to 100 GHz. A Gaussian window in the time domain is applied to limit the maximum frequency content of the excitation to prevent numerical aliasing in the computation of the response. The shape of the Gaussian window and its frequency characteristics are shown on Figure 6. Figure 7 shows the backward scattered field of the wire after windowing the transient response. The time-domain response due to the backward

scattered field is obtained by evaluating an inverse Fourier transform (FFT) of the Gaussian windowed frequency domain data, which is the solid line of Figure 8. The sampling frequency used is 4 times the highest frequency of interest. The expansion coefficients of the associate Hermite polynomials used to fit the transient data in Figure 8 is obtained by using Equation (21). They are displayed in Figure 9. The order of the associate Hermite polynomial expansion is determined by the time-bandwidth product (2BT+1) rule, where B is the one-sided bandwidth in the frequency domain and T is the time duration of the signal. This implies that to approximate the waveform of duration T and which is practically band limited to B, by using an orthonormal set of basis functions in the time domain, at least (2BT+1) pieces of basis are necessary from a mathematical point of view. In this example the frequency band B is 100 GHz and the total time duration T is 5 nsec. Therefore, to achieve this time-bandwidth product for the backward scattered field one needs approximately N = (2 x 100 x 5 + 1) = 1001 coefficients of the Hermite expansion as shown in Figure 9 are necessary to approximate the waveform in either in the time or in the frequency domain.

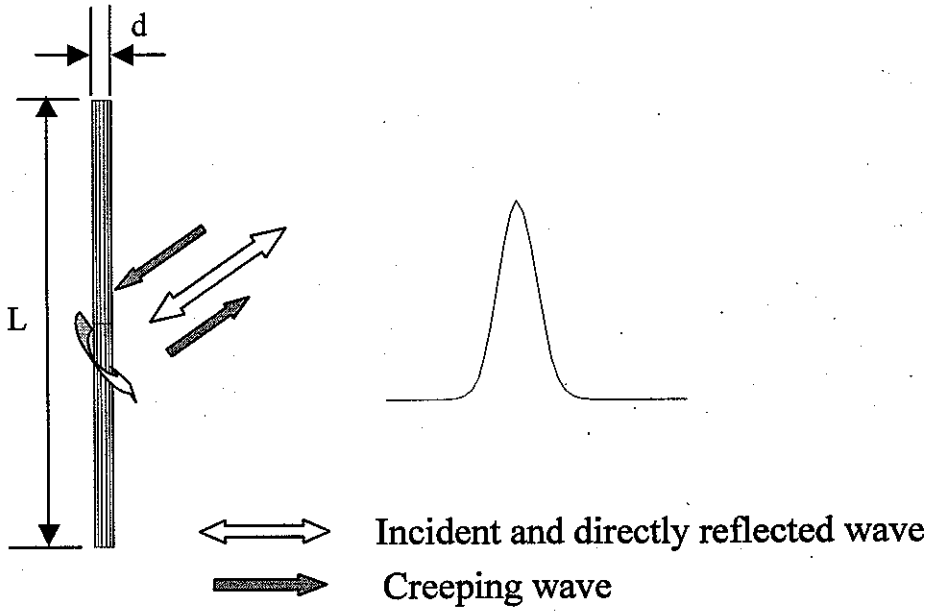

Figure 4. A wire scatterer radiated by an incident wave from the broadside direction.

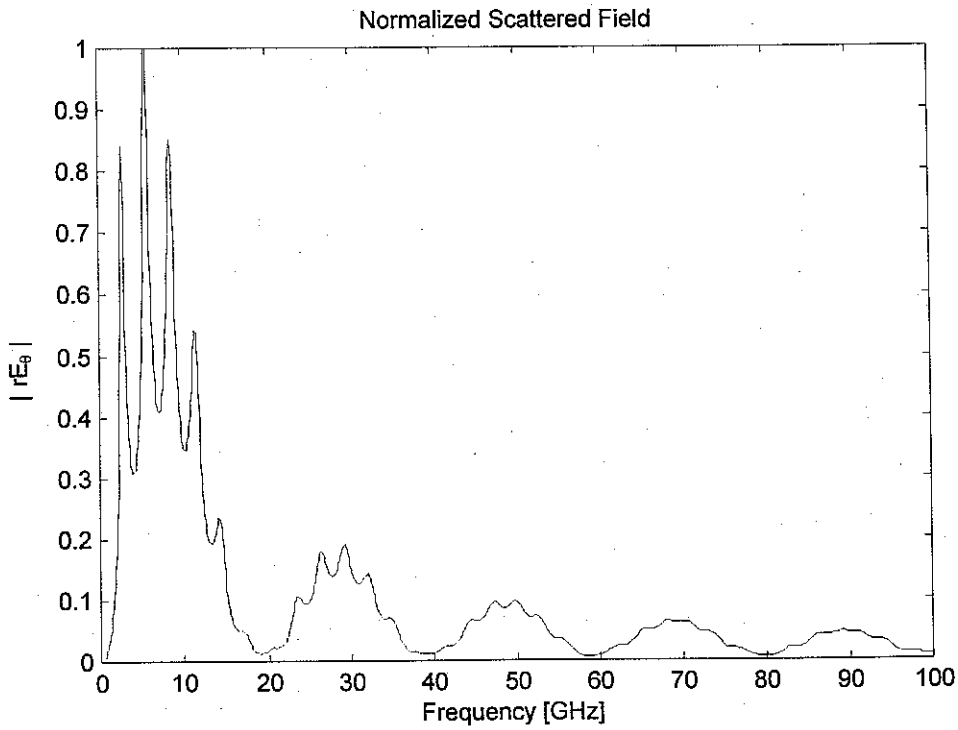

Figure 5. Normalized back scattered field calculated using WIPL-D.

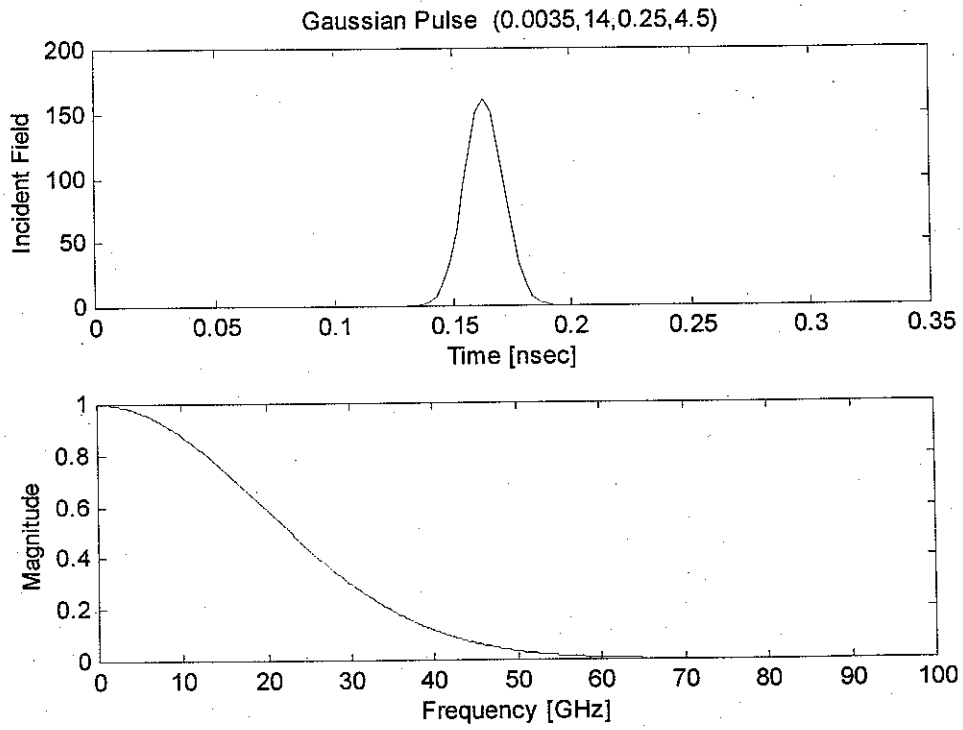

Figure 6. A Gaussian pulse in the time domain and its spectrum.

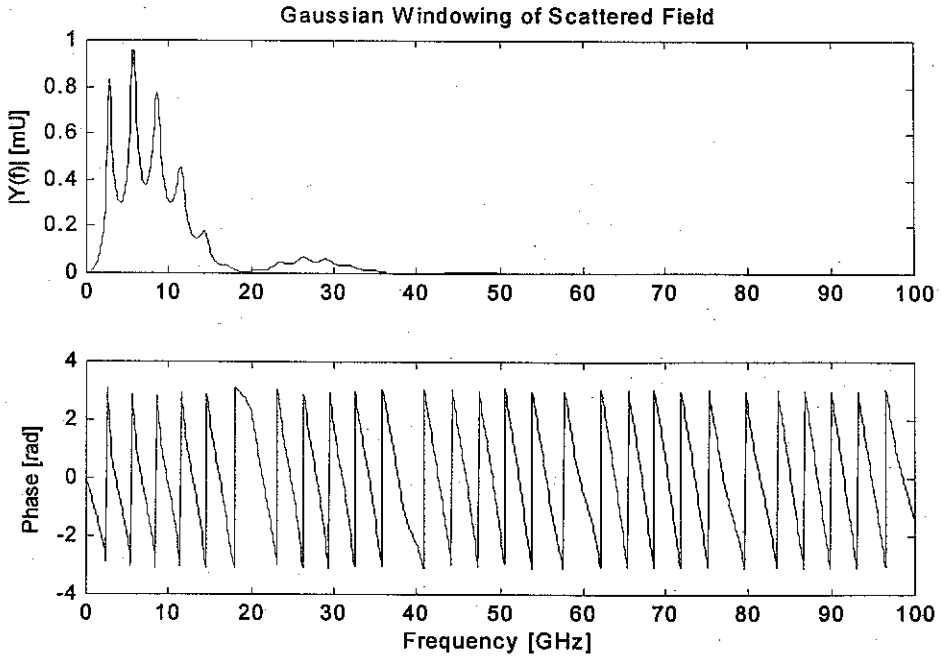

Figure 7. The back scattered fields obtained after windowing the transient response.

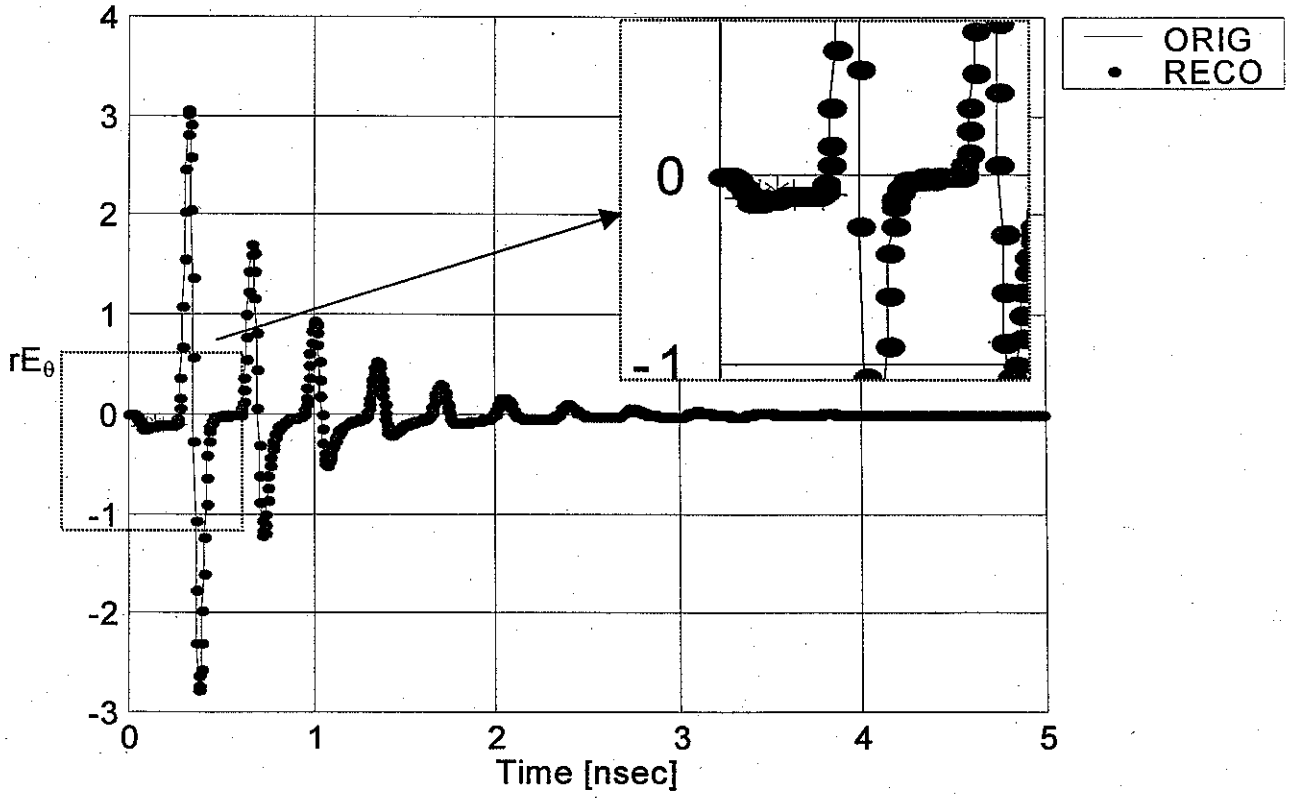

Figure 8. Backward scattered field of a wire scatterer in the time domain (Dot is the reconstructed signal using the optimized parameters).

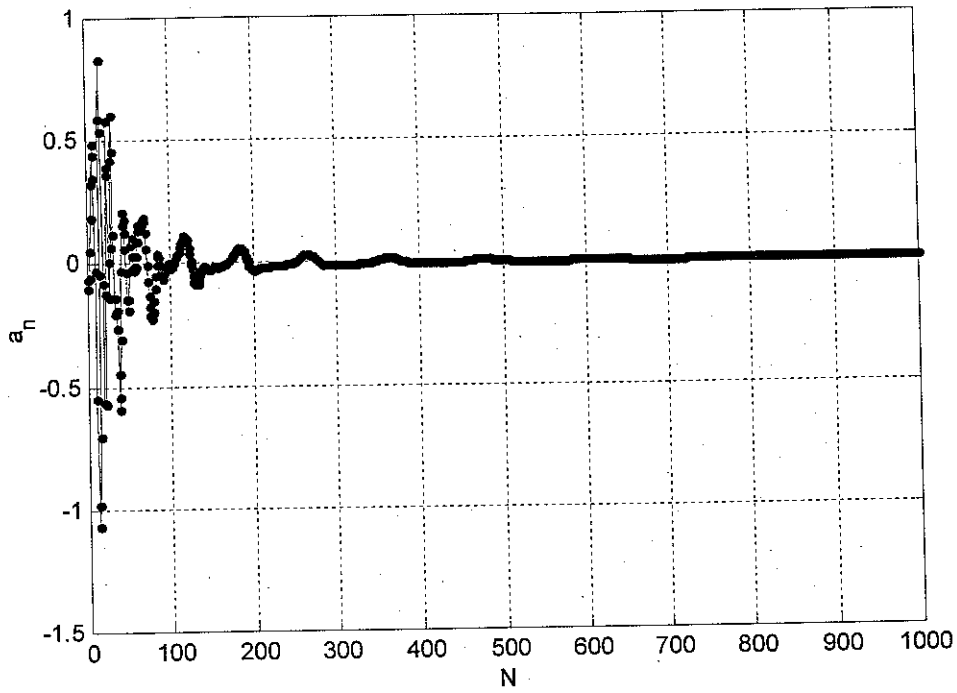

Figure 9. Expansion coefficients of the Associate Hermite functions approximating the time domain function.

In order to start the optimization process to estimate the parameters of interest a good initial guesses of the complex exponents related to the poles are obtained by applying the matrix pencil method on the late time data, which covers from the 5.5% to 99% of the data set, shown in Figure 8. The number of poles is obtained from the singular value decomposition of the data as required in the Matrix Pencil method. A threshold is applied to the relative magnitudes of the singular values as shown in Figure 10 to separate the signal poles from the noise ones. The y-axis of Figure 10 is in dB scale and the straight line represents a threshold to distinguish the signal poles from the noise ones. From the application of the threshold only fourteen large singular values are chosen which corresponds to seven poles.

The half Fourier transform of the time domain signal is calculated using (44) by using the associate Hermite expansion coefficients of Figure 9, which is shown by the solid line in Figure 11. By using the backward scattered field and the HFT of the signal, one can now optimize the set of parameters related to the Gaussian pulse-like functions and the complex

exponentials. The reconstructed time domain and HFT domain signal are shown by dots in the Figures 8 and 11.

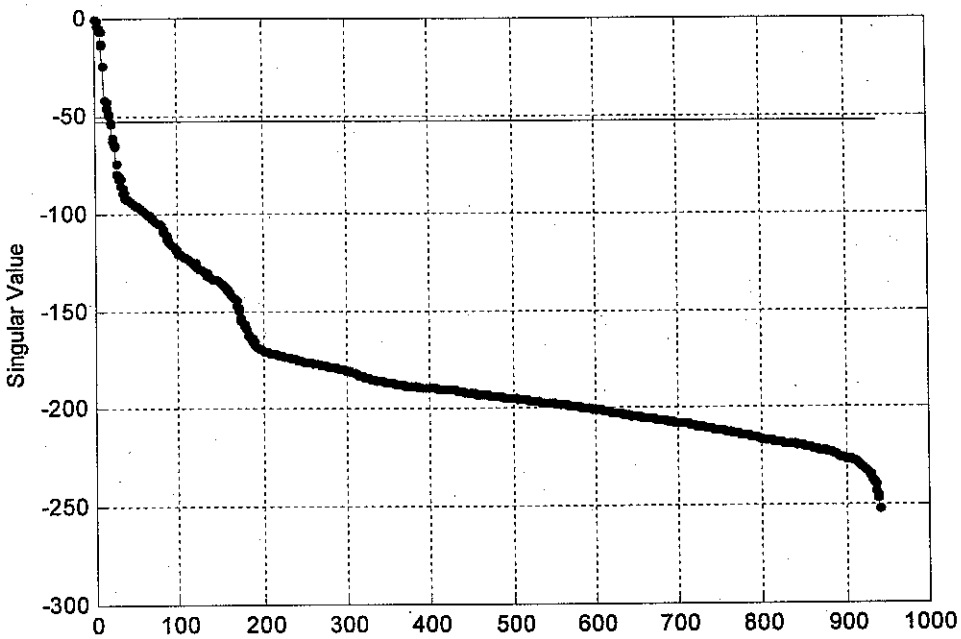

Figure 10. Ratio of the Singular values σ_i/σ_{max} in a dB scale.

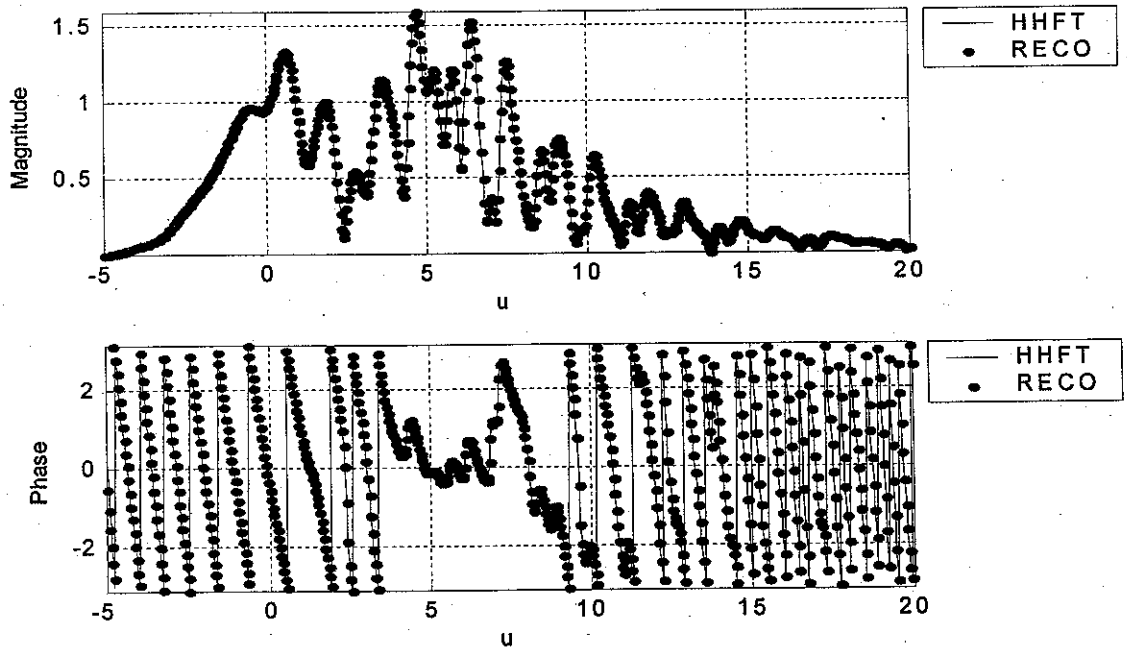

Figure 11. Plot of the signals in the half Fourier transform (HFT) domain. (Dots are the reconstructed signals with the optimized parameters).

To represent the early time part, 5 Gaussian-shaped- pulses are used, that are shown by an asterisk (*) in the insert of Figure 8. The number of pulses is less than the possible number of creeping waves in this case. The Root mean square error (RMSE) associated with the reconstruction of the time domain signal and the HFT domain signal are 0.0032 and 0.0035, respectively. The pole locations in the complex s-plane are plotted in Figure 12. The x-axis represents the normalized damping coefficient and the y-axis is the normalized frequency. In the labels associated with both the axes in Figure 12, L is the length of the wire scatterer and c is the velocity of light. The analytical data for the complex poles has been presented by Tesche [32]. It shows that, the frequency components of the computed poles coincide well with the analytic data, but the damping components display some differences.

Next we apply this procedure to the data obtained from a conducting sphere.

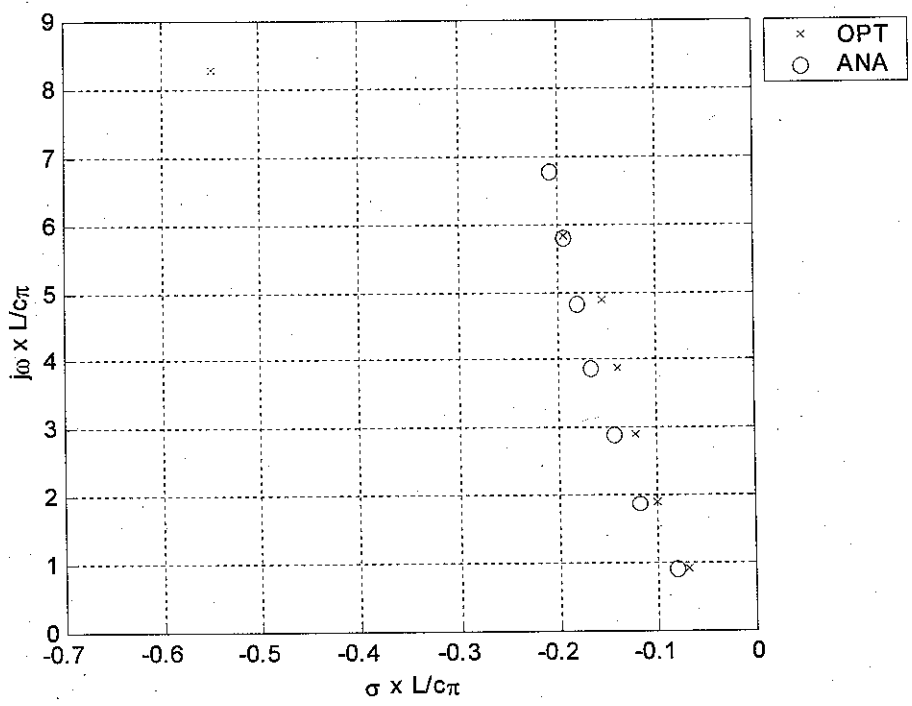

Figure 12. Locations of the poles for the wire scatterer.

5.2 A conducting sphere

The second example considered is a conducting sphere of radius 1cm, which is shown in Figure 13. The back-scattered field has been computed using the electromagnetic analysis code WIPL-D in the frequency domain, as shown in Figure 14. The incident field is coming from the top and is x-polarized. A Gaussian window is applied in the time domain to limit the spectral bandwidth of the incident waveform. The inverse Fourier transformed frequency domain data is shown in Figure 15 by a solid line. This data exhibits two types of pulses. One is a directly reflected pulse and another is a creeping wave. The time difference between these two pulses is about 0.176ns. This shows a good agreement with the calculated value of 0.1714ns. $\{(2+\pi)\times r/3x10^8 = 0.1714\,\text{nsec}\}$. Figure 16 shows the plot of the coefficients of the associate Hermite (AH) polynomials used to approximate the time domain waveform. The order of the associate Hermite polynomials (AH) is determined using the time-bandwidth product rule of 2BT+1. In this example the frequency band B is 100 GHz and the time duration T is 0.65 nsec. So in this case N = 2×100 ×0.65 + 1 = 131. However, a larger value for N = 301 has been chosen to guarantee convergence of the solution.

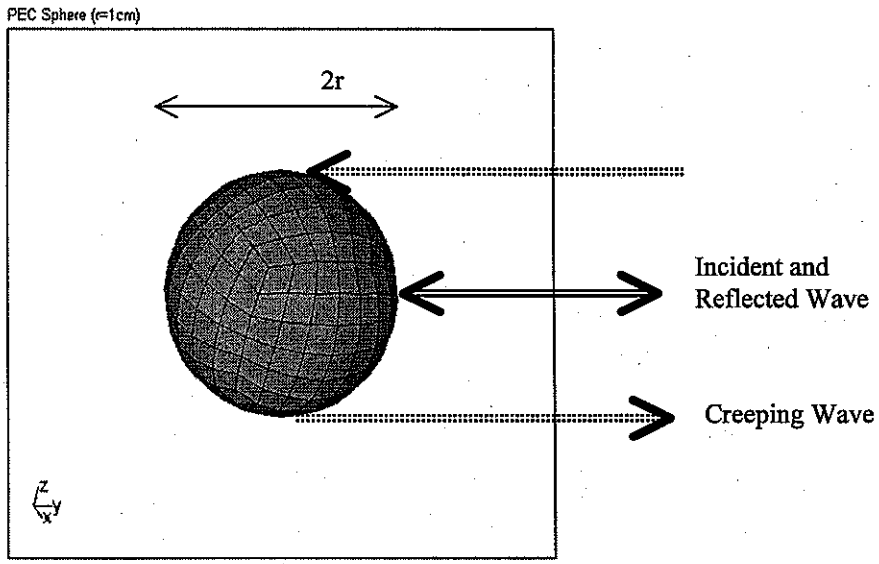

Figure 13. A conducting sphere.

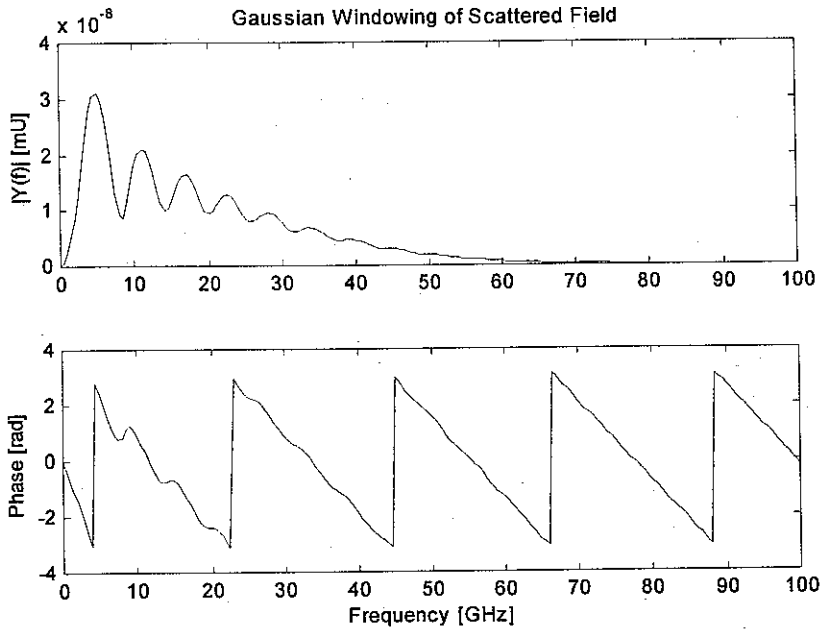

Figure 14. Back Scattered field after applying a Gaussian window to the time domain data.

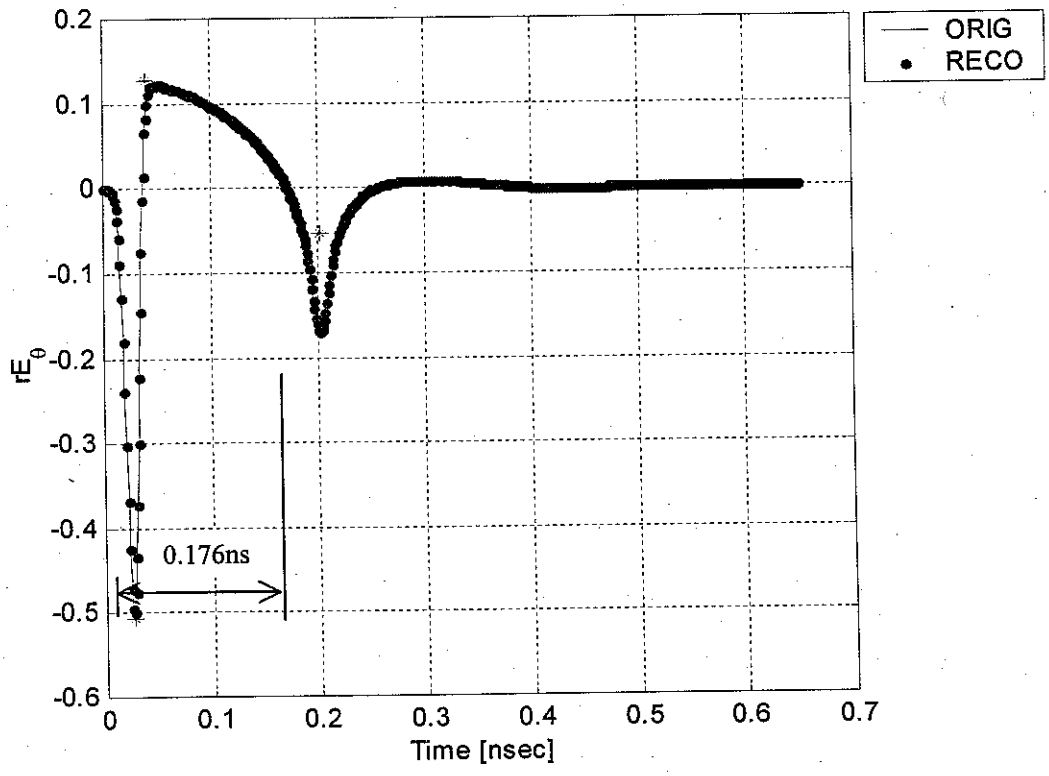

Figure 15. Back scattered field of a conducting sphere in the time domain.

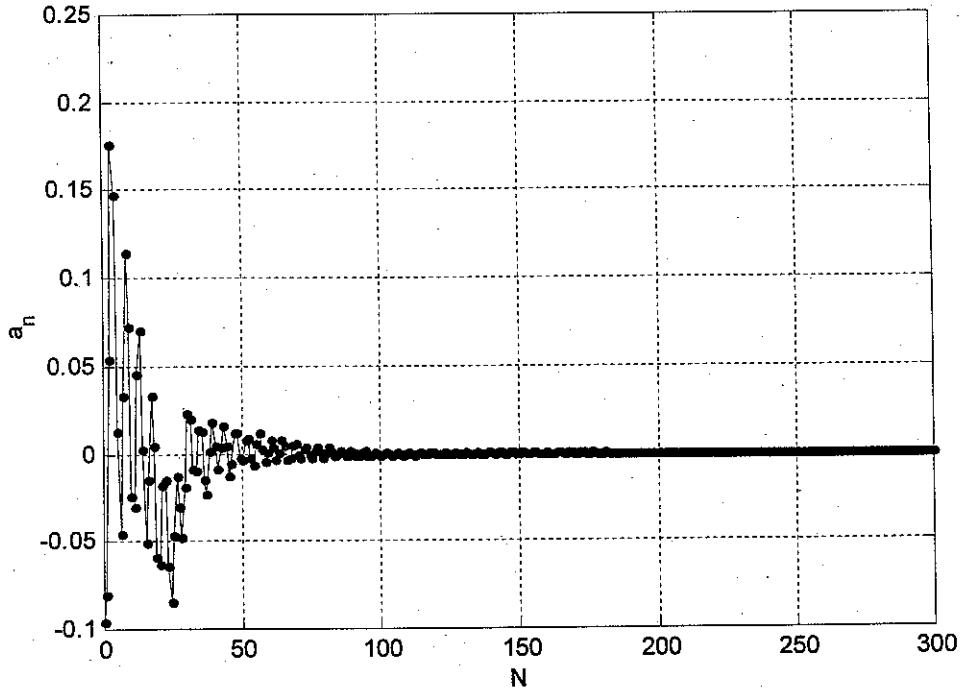

Figure 16. Expansion coefficients of the Associate Hermite functions in approximating the time domain signal.

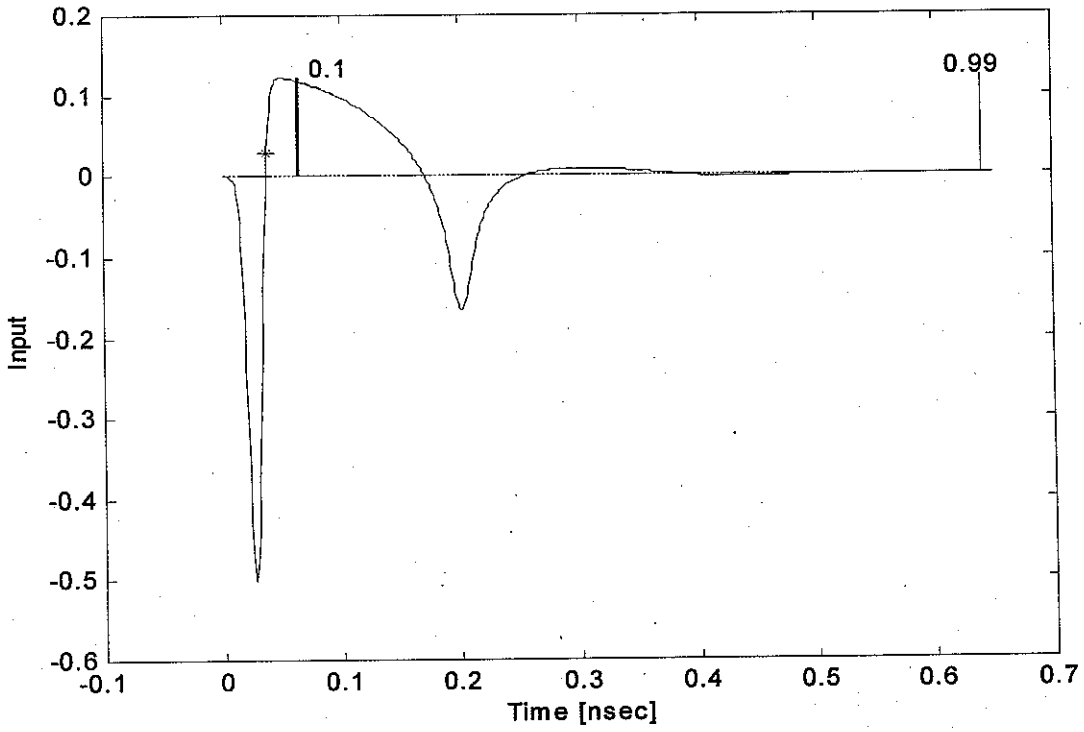

Figure 17. Portions of the input data used in matrix pencil method (from 10% to 99%). (Asterisk represents the initial value of the turn-on time)

Initial guesses for the complex exponentials are obtained using the Matrix Pencil method by using the time domain data, extending from 10% to 99% of its original value as shown in Figure 17. It is clear that there is one creeping wave in this range, so there may be some difficulty when we use the matrix pencil method. With the comparison of the computed singular values to the largest one in magnitude, as shown in Figure 18, 26 poles, or equivalently 52 singular values, are chosen. But we know that there is apparently one creeping wave in the region. However, due to the presence of the creeping wave the power or equivalently the amplitude associated with the all the complex poles are also taken into consideration. By using the power as a metric for comparison, we reevaluate the number of dominant poles. The average power is calculated by taking the time average of the amplitude for each complex exponential. If the power associated with the exponentials is greater than 0.1% of the total average power of the signal then they are retained in the computation. As a result, 21 poles are selected, which are shown in Figure 19. The solid line in Figure 20 shows the half Fourier transform of the backward scattered field, which is calculated using the coefficients of the associate Hermite functions. Parameter optimization is performed simultaneously in the HFT domain and in the time domain to select the optimum set of parameters of the Gaussian-like impulses and the decaying exponentials. In this example, 3 Gaussian pulses have been obtained which are used to represent the early-time signal. Those pulses are shown by an asterisk (*) in Figure 15. The asterisks represent the amplitude and position of the pulses. It appears that there is a pulse doublet. This is due to the derivative of the incident Gaussian pulse. The third one is the creeping wave. Another creeping wave can be found around 0.4 nsec but its amplitude is very small.

The reconstructed time domain and HFT domain signals using the associate Hermite polynomials are shown in Figures 15 and 20 by the dots. The root mean square error in the approximation of the waveform in the time domain is 0.0036 and that in the HFT domain is 0.0026. Figure 21 shows the estimated pole locations along with the analytic values. The analytical data for the poles have been obtained from [34]. In Figure 21, a is the radius of the sphere and c is the velocity of light. They show good agreement even for the damping constants.

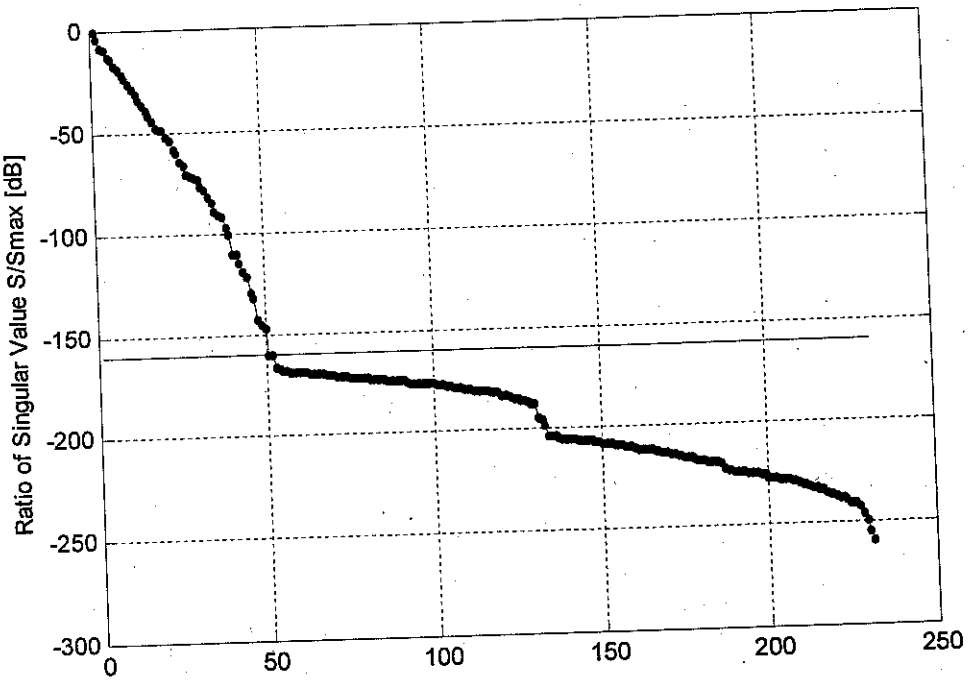

Figure 18. Ratio of the Singular values σ_i / σ_{max} in dB scale (Strait line is the threshold)

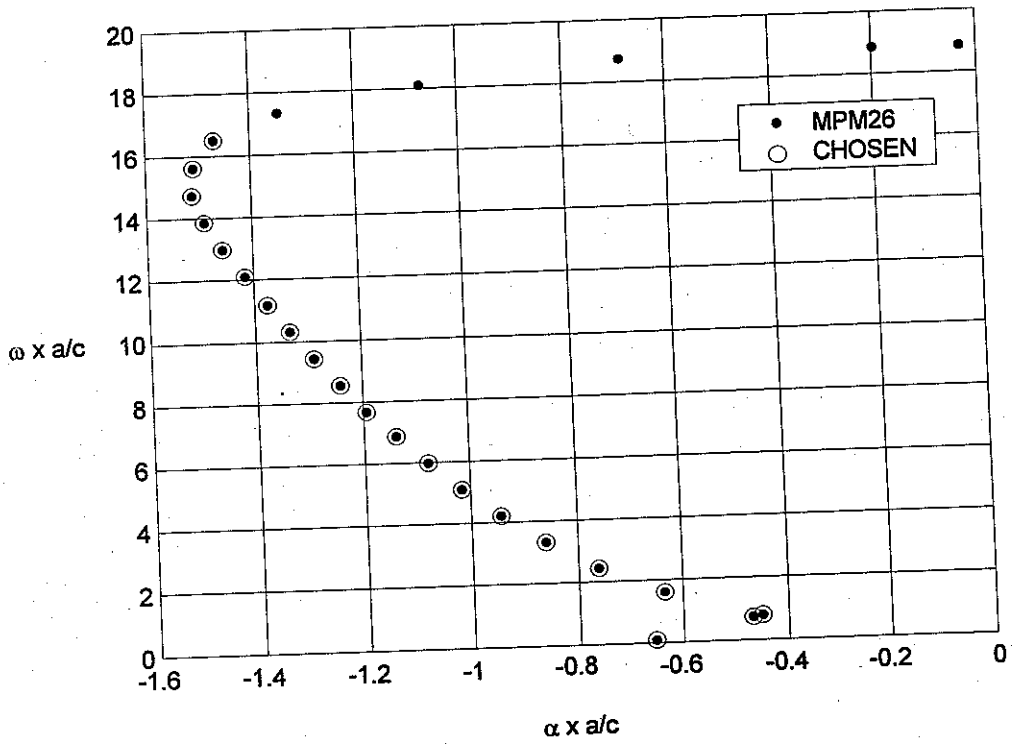

Figure 19. Initial guesses of the exponentials using the Matrix Pencil method for the conducting sphere. (Circled points represent the pole locations after using the power criterion)

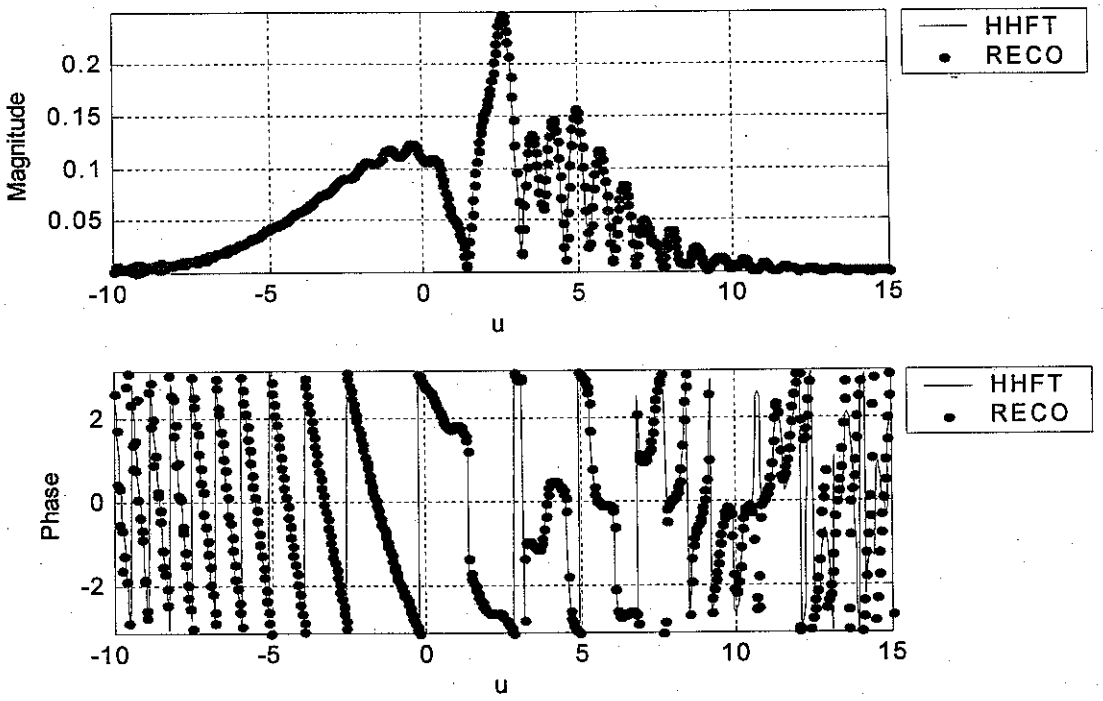

Figure 20. Half Fourier Transform (HFT) of the signals.
(Dot is the reconstructed signal using the optimized parameters.)

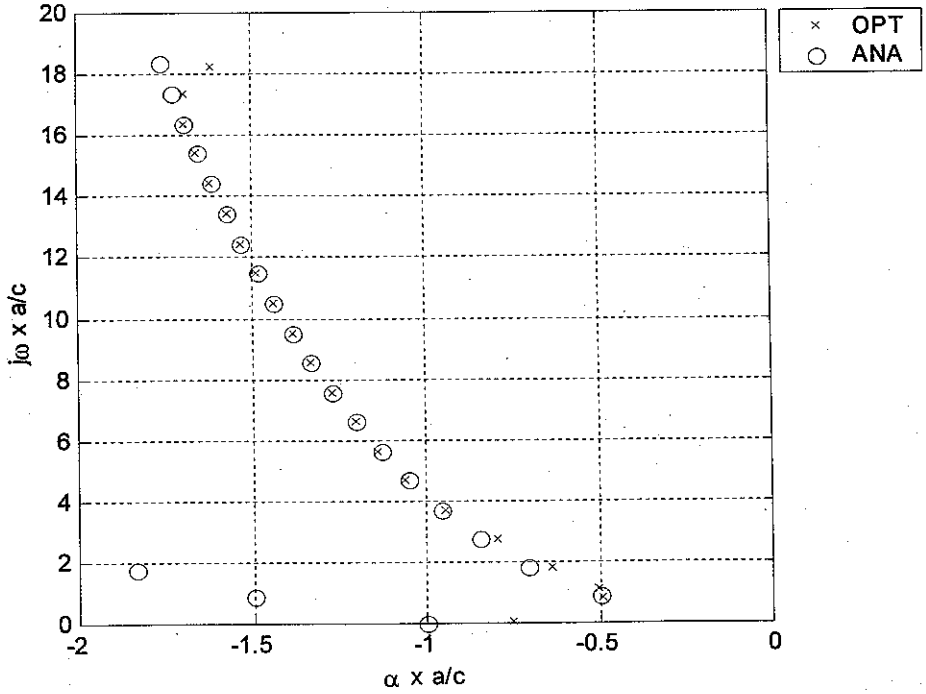

Figure 21. Pole locations for the conducting sphere.

6. Conclusions

A new technique is presented for extracting the parameters of the damped sinusoids and the early time impulse like responses using the entire transient response data set. Hence, the time domain data contains both the early time and late time responses. Early time responses have pulse-like components and this makes it hard to analyze the complete signal. In this study, Guassian pulses have been used to describe the early time portion of the data and a fractional Fourier transform is used to separate the pulse like components from the damped exponentials. Initial guess for the complex exponentials using the Matrix Pencil method gives us a good starting point for the optimization process. We show that the Half Fourier Transform is very effective when the transient response from a target has pulse-like components. The results for the wire scatterer and conducting sphere show that the proposed technique performs well in extracting the aspect independent complex resonance information of the object. Analytical results from the references [32-34] show that there are multiple layers of poles but during this study we could observe the poles only from the first layer. They are quite adequate to represent the transient responses from various objects. A parameter optimization to match both the transient and the half Fourier transform data shows that an individual exponential function has their own 'turn-on time' which will be described in details in the next paper.

7. REFERENCES

[1] E. M. Kennaugh and D. L. Moffatt, "Transient and impulse response approximations," *Proc. EEE*, Vol. 53, pp. 893-901,Aug. 1965.

[2] A. A. Ksienski, Y. Lin, and L. J. White, "Low frequency approach to target identification," *Proc. IEEE*, Vol. 63, No. 12, pp. 1651-1660, Dec. 1975.

[3] J. D. Young, "Radar imaging from transient response signatures," *IEEE Trans. Antennas Propagat.*, Vol. 24, No. 3, pp. 276-282, May 1976.

[4] L. C. Chan, D. L. Moffatt, and L. Peters, "A characterizaton of subsurface radar targets," *Proc. IEEE*, Vol. 67, No. 7, pp. 991-1000, July 1979.

[5] C. E. Baum, "On the singularity expansion method for the solution of electromagnetic interaction problems", *Interaction Note 88*, Air Force Weapons Lab, Dec. 1971.

[6] C. E. Baum, "Emerging technology for transient and broad-band analysis and synthesis of antenna and scatterers," *Proc. IEEE*, Vol. 64, No. 11, pp. 1598-1616, Nov. 1976.

[7] D. L. Moffatt and R. K. Mains, "Detection and discrimination of radar targets," *IEEE Trans. Antennas Propagat.*, Vol. AP-23, No. 3, pp. 358-367, May 1975.

[8] M. L. VanBlaricum and R. Mittra, "A technique for extracting the poles and residues of a system directly from its transient response," *IEEE Trans.Antennas,Propagat.*, Vol. AP-23, No. 6, pp.777-781, 1975.

[9] E. K. Miller, "Natural mode methods in frequency and time domain analysis," in *Theoretical methods for determining the interaction of electromagnetic waves with structures*, Sijthoff and Noordhoff, Netherlands, 1981.

[10] A. J. Poggio, M. L. Van Blaricum, E. K. Miller, R. Mittra, "Evaluation of a processing technique for transient data," *IEEE Trans. Antennas and Propagat.* , Vol. AP-26, No. 1, pp. 165-173, Jan., 1978.

[11] R. Kumaresan, "Estimating the parameters of exponentially damped or undamped sinusoidal signals in noise," Ph.D. dissertation, Univ of Rhode Island, 1982.

[12] Y. Hua and T. K. Sarkar, "Further analysis of three modern techniques for poles retrieval from data sequence," in *Proc. 30th Midwest Sympo. Circuits Syst.*, Aug. 1987, Syracuse, NY.

[13] Y. Hua and T.K. Sarkar, "Perturbation analysis of TK method for harmonic retrieval problems," *IEEE trans. Acoust., Speech signal processing*, Vol. ASSP-36, No. 2, pp. 228-240, Feb. 1988 .

[14] T. K. Sarkar, J. Nebat, D. D. Weiner, and V. K. Jain, "Suboptimal approximation/identification of transient waveforms from electromagnetic systems by pencil of function method," *IEEE Trans .Antennas and Propagat.*, Vol. AP-28, No. 6, pp. 928-933, Nov. 1980.

[15] A. J. Mackay and A. McCowen, "An improved pencil of functions method and comparisons with traditional methods of pole extraction," *IEEE Trans. Antennas and Propagation,* Vol. AP-35, No. 4, pp. 435-441, Apr. 1987.

[16] Y. Hua and T.K.Sarkar, "Generalized pencil-of-functions method for extracting the pole of an electromagnetic system from its transient response," *IEEE Trans. Antennas and Propagat.,* Vol. 37, No. 2, pp. 229-234, Jan., 1989.

[17] L. W. Pearson, "A note on the representation of scattered fields as a singularity expansion," *IEEE Trans. Antennas and Propagat.*, Vol. AP-32, No. 5, pp. 520-524, May, 1984.

[18] M. A. Morgan, "Singularity expansion representations of fields and currents in transient scattering," *IEEE Trans. Antennas and Propagat.*, Vol. AP-32, No. 5, pp. 466-473, May, 1984.

[19] I. S. Gradshteyn and I. M. Ryzhik, " *Table of Integrals, series and products*", Academic Press, p. 307, 1980.

[20] V. Namias, "The fractional order Fourier transform and its application to quantum mechanics", *J. Inst. Math. Applic.*, Vol. 25, pp. 241-265,1980.

[21] L. B. Felsen, "Comments on early time SEM," *IEEE Trans. Antennas and Propagat.,* Vol. AP-33, No. 1, pp.118-119, Jan. 1985.

[22] C. E. Baum, "Representation of surface current and far scattering in EEM and SEM with entire functions," *Interaction Note, 486,* Air Force Weapons Lab, Dec. 1971; Chapter 13, pp. 273-316, P. P. delSanto and A.W. Saenz (eds.), *New perspectives on problems in classcal and quantum physics, Pt. II, Acoustic Propagation and Scattering , Electromagnetic Scattering*, Gordon and Breach, 1998.

[23] E. Heyman and L. B. Felsen, "A wavefront interpretation of the singularity expansion method," *IEEE Trans. Antennas and Propagat.*, Vol. AP-33, No. 7, pp. 706-718, July, 1985.

[24] G. L. James, Geometrical theory of diffraction for electromagnetic waves, 3rd ed., London, Peter Peregrinus, 1986.

[25] E. Heyman and L.B. Felsen, "Wavefront interpretation of SEM resonances, turn-on time, and entire functions," *Hybrid formulation of wave propagation and scattering*, L.B. Felsen Ed. The Hague, Netherlands, Nijhoff, 1984, pp. 253-267.

[26] A. C. McBride, F. H. Kerr, "On Namias's fractional Fourier transforms",*IMA J. Appl.Math*, Vol. 39, pp. 159-175,1987.

[27] L. B. Almeida, "The fractional Fourier transform and time-frequency representations", *IEEE Trans. On Signal Processing*, Vol. 42, No. 11, pp. 3084-3091, 1984.

[28] L. R. Conte, R. Merletti, G. V. Sandri, "Hermite expansions of compact support waveforms: applications to myoelectric signals", *IEEE Trans. on Biomedical Engineering*, Vol. 41, No.12, Dec. 1994.

[29] Y. Hua and T. K. Sarkar, "Matrix pencil method for estimating parameters of exponentially damped/undamped sinusoids in noise", *IEEE Trans on Acoustics, Speech, and Signal Processing*, Vol. 38, No. 5, pp. 814-824,1990.

[30] T. K. Sarkar and Odilon Pereira, "Using the Matrix Pencil Method to estimate the parameters of a sum of complex exponentials", *IEEE Antennas and Propagation Magazine*, Vol. 37, No. 1, pp. 48-55, 1995.

[31] B. M. Kolundzija, J. S. Ognjanovic and T. K. Sarkar, " *WIPL-D* (for Windows manual)", Artech House, Norwood, mass., 2000.

[32] F. M. Tesche, "On the Analysis of Scattering and Antenna Problems Using the Singularity Expansion Technique," *IEEE Trans. On Antennas and Propagat.*, Vol. AP-21, No. 1, pp. 53-62, 1973.

[33] C. Baum, " An observation concerning the entire function in SEM cattering", Interaction Note 567, 2001.

[34] K. M. Chen and D. Westmoreland, "Impulse response of a conducting sphere based on singularity expansion method," *Proc. IEEE*, Vol. 69, No. 6, pp. 747-750, 1981.